



Multiparametric MR-PET Imaging Predicts Pharmacokinetics and Clinical Response to GDC-0084 in Patients with Recurrent High-Grade Glioma

Benjamin M. Ellingson^{1,2,3,4,5,6}, Jingwen Yao^{1,2,3}, Catalina Raymond^{1,2}, David A. Nathanson⁷, Ararat Chakhoyan^{1,2}, Jeremy Simpson⁸, James S. Garner⁸, Alan G. Olivero⁹, Lars U. Mueller⁹, Jordi Rodon¹⁰, Elizabeth Gerstner¹¹, Timothy F. Cloughesy^{6,12}, and Patrick Y. Wen¹³

ABSTRACT

Purpose: GDC-0084 is an oral, brain-penetrant small-molecule inhibitor of PI3K and mTOR. Because these two targets alter tumor vascularity and metabolism, respectively, we hypothesized multiparametric MR-PET could be used to quantify the response, estimate pharmacokinetic (PK) parameters, and predict progression-free survival (PFS) in patients with recurrent malignant gliomas.

Patients and Methods: Multiparametric advanced MR-PET imaging was performed to evaluate physiologic response in a first-in-man, multicenter, phase I, dose-escalation study of GDC-0084 (NCT01547546) in 47 patients with recurrent malignant glioma.

Results: Measured maximum concentration (C_{max}) was associated with a decrease in enhancing tumor volume ($P = 0.0287$) and an increase in fractional anisotropy (FA; $P = 0.0418$). Posttreatment tumor volume, ^{18}F -FDG uptake, K^{trans} , and rel-

ative cerebral blood volume (rCBV) were all correlated with C_{max} . A linear combination of change in ^{18}F -FDG PET uptake, apparent diffusion coefficient (ADC), FA, K^{trans} , v_p , and rCBV was able to estimate both C_{max} ($R^2 = 0.4113$; $P < 0.0001$) and drug exposure (AUC; $R^2 = 0.3481$; $P < 0.0001$). Using this composite multiparametric MR-PET imaging response biomarker to predict PK, patients with an estimated $C_{max} > 0.1 \mu\text{mol/L}$ and AUC $> 1.25 \mu\text{mol/L} \cdot \text{hour}$ demonstrated significantly longer PFS compared with patients with a lower estimated concentration and exposure ($P = 0.0039$ and $P = 0.0296$, respectively).

Conclusions: Results from this study suggest composite biomarkers created from multiparametric MR-PET imaging targeting metabolic and/or physiologic processes specific to the drug mechanism of action may be useful for subsequent evaluation of treatment efficacy for larger phase II–III studies.

Introduction

Glioblastoma is a complex disease with a dismal prognosis of only 12–21 months from initial diagnosis when treated with maximal safe

resection followed by radiotherapy combined with temozolomide plus adjuvant temozolomide with or without tumor-treating fields (1–3). Despite aggressive initial therapy, almost all patients with glioblastoma relapse and after first-line treatment failure there are limited treatment options for glioblastoma.

The Cancer Genome Atlas (TCGA) has identified the PI3K pathway as one of the most frequently altered pathways, being mutated, amplified, or having loss of signaling proteins in more than 80% of human glioblastomas (4). While most drugs that inhibit the PI3K/Akt/mTOR pathway have not achieved favorable results, including erlotinib (5), lapatinib (6), everolimus (7), and gefitinib (8, 9), this was largely attributed to the inability of these compounds to adequately cross the blood–brain barrier (10–13), resulting in subtherapeutic concentrations within the tumor. 5-(6,6-Dimethyl-4-morpholino-8,9-dihydro-6H-[1,4]oxazino[4,3-e]purin-2-yl)pyrimidin-2-amine (GDC-0084) is a selective inhibitor of PI3K and mTOR specifically optimized for brain penetration and developed as a potential treatment of glioblastoma (14). Preclinical studies have shown the ability for GDC-0084 to inhibit the proliferation of several glioma cell lines, and careful molecular imaging studies have demonstrated adequate penetration of GDC-0084 within intracranial tumors (14, 15). These results suggest GDC-0084 may be efficacious in glioblastoma.

From 2012–2014 an open-label, phase I, dose-escalation study was performed in patients with recurrent high-grade gliomas in order to assess the safety and tolerability of GDC-0084. The safety and tolerability were described previously (16). Because of the metabolic consequences of mTOR inhibition (17–19) and the known role of PI3K in angiogenesis (20–22), we hypothesized higher concentrations of GDC-0084 within the brain would result in proportional reductions in both glucose utilization and tumor vascularity. We rationalized that

¹UCLA Brain Tumor Imaging Laboratory (BTIL), Center for Computer Vision and Imaging Biomarkers, University of California, Los Angeles, Los Angeles, California. ²Department of Radiological Sciences, David Geffen School of Medicine, University of California, Los Angeles, Los Angeles, California. ³Department of Bioengineering, Henry Samueli School of Engineering and Applied Science, University of California, Los Angeles, Los Angeles, California. ⁴Department of Psychiatry and Biobehavioral Sciences, David Geffen School of Medicine, University of California, Los Angeles, Los Angeles, California. ⁵Brain Research Institute, David Geffen School of Medicine, University of California, Los Angeles, Los Angeles, California. ⁶UCLA Neuro-Oncology Program, University of California, Los Angeles, Los Angeles, California. ⁷Department of Molecular and Medical Pharmacology, David Geffen School of Medicine, University of California, Los Angeles, Los Angeles, California. ⁸Kazia Therapeutics Limited, Sydney, New South Wales, Australia. ⁹Genentech, Inc., South San Francisco, California. ¹⁰Vall d'Hebron Institute of Oncology, Barcelona, Spain. ¹¹Department of Neurology, Massachusetts General Hospital, Boston, Massachusetts. ¹²Department of Neurology, David Geffen School of Medicine, University of California, Los Angeles, Los Angeles, California. ¹³Center for Neuro-Oncology, Dana-Farber Cancer Institute, Harvard Medical School, Boston, Massachusetts.

Note: Supplementary data for this article are available at Clinical Cancer Research Online (<http://clincancerres.aacrjournals.org/>).

Corresponding Author: Benjamin M. Ellingson, David Geffen School of Medicine at UCLA, 924 Westwood Blvd., Suite 615, Los Angeles, CA 90024. Phone: 310-481-7572; Fax: 310-794-2796; E-mail: bellingson@mednet.ucla.edu

Clin Cancer Res 2020;XX:XX–XX

doi: 10.1158/1078-0432.CCR-19-3817

©2020 American Association for Cancer Research.

Translational Relevance

While questions regarding brain penetration and target engagement in experimental therapies are typically answered using early-phase surgical studies, an alternative strategy is to use advanced imaging to quantify downstream physiologic changes that are theorized to change as a result of target engagement. This study demonstrates that a combination of MRI and PET imaging can predict pharmacokinetic parameters and progression-free survival of recurrent malignant gliomas treated with GDC-0084, an oral, brain-penetrant small-molecule inhibitor of PI3K and mTOR, likely due to the metabolic consequences of mTOR inhibition and the known role of PI3K in angiogenesis and proliferation. Results from this study suggest multiparametric MR-PET imaging targeting biologic processes specific to the drug mechanism of action may be useful for evaluation of treatment efficacy for larger phase II–III studies.

because GDC-0084 is a brain-penetrant agent, pharmacokinetics (PK) would be related to tissue pharmacodynamics (PD) and, therefore, target engagement resulting in physiologic changes would only result when PK parameters were favorable. Thus, this study examined the dose-dependent, multiparametric MRI and PET imaging response in this “first-in-man” study to document traditional radiographic response as well as determine whether advanced MR or PET imaging techniques could predict drug PK parameters and progression-free survival (PFS).

Patients and Methods

Patients and study design

A classical “3 + 3” design was used to assess safety, tolerability, and pharmacokinetics of GDC-0084 administered orally once daily in

patients with recurrent high-grade glioma in this open-label, multi-center, Phase I, dose-escalation study (NCT01547546). A total of 47 patients with recurrent or progressive high-grade gliomas were enrolled in the Stage 1 (dose escalation) portion of this study in four sites in the United States and Europe [University of California Los Angeles (Los Angeles, CA), Dana Farber Cancer Institute (Boston, MA), Massachusetts General Hospital (Boston, MA), and Hospital Universitario Vall d'Hebron Institute of Oncology (Barcelona, Spain)]. Of these patients, 13 (27.7%) were female and 34 (72.3%) were male. Patients were predominantly white (93.6%) and predominately not of Hispanic or Latino origin (93.6%). The mean age of patients was 49.7 years (range 29–73 years) at baseline. Patients received a dose of 2 mg ($N = 7$), 4 mg ($N = 4$), 8 mg ($N = 5$), 15 mg ($N = 6$), 20 mg ($N = 4$), 30 mg ($N = 7$), 45 mg ($N = 8$), or 65 mg ($N = 6$) of study drug. Patient characteristics are highlighted in **Table 1**.

All patients who received GDC-0084 were over age 18, signed conformed consent forms at their local sites to contribute to this study, had a life expectancy >12 weeks from enrollment, and histologically documented recurrent or progressive high-grade gliomas (WHO III–IV gliomas) with Karnofsky performance status ≥ 70 at screening who were at least 12 weeks from completion of concurrent chemoradiation (radiotherapy + concurrent temozolomide). In addition, all patients included in this trial had <2 mg dexamethasone per day or an equivalent dose of other systemic anti-inflammatory corticosteroid or immunosuppressant prior to enrollment. Additional inclusion and exclusion criteria can be found at (<https://clinicaltrials.gov/ct2/show/NCT01547546>) and in the published clinical details of the trial (23).

The study protocol was approved by local Institutional Review Boards prior to patient recruitment and was conducted in accordance with the Declaration of Helsinki International Conference on Harmonization E6 Guidelines for Good Clinical Practice. Written informed consent was obtained for all patients prior to performing study-related procedures in accordance with federal and institutional guidelines.

Table 1. Patient demographics.

Demographic characteristics	2 mg ($N = 7$)	4 mg ($N = 4$)	8 mg ($N = 5$)	15 mg ($N = 6$)	20 mg ($N = 4$)	30 mg ($N = 7$)	45 mg ($N = 8$)	65 mg ($N = 6$)	All patients ($N = 47$)
Age (years)									
Mean (SD)	53.7 (10.5)	54.0 (16.1)	46.2 (8.0)	53.2 (10.2)	39.0 (10.5)	58.0 (9.8)	47.0 (10.5)	42.7 (11.7)	49.7 (11.6)
Median	58	61	44	57	38	56	48.5	41.5	50
Range	32–63	30–64	38–59	38–62	30–50	44–73	31–62	29–59	29–73
Sex (F/M)	2/5	1/3	0/5	2/4	4/3	4/3	2/6	0/6	13/34
Race									
Asian	0	0	0	0	1	0	0	0	1
White	7	4	5	6	2	7	8	5	44
Other	0	0	0	0	1	0	0	1	2
Ethnicity									
Hispanic or Latino	0	0	0	1	1	0	0	1	3
Not Hispanic or Latino	7	4	5	5	3	7	8	5	44
Baseline weight (kg)									
Mean (SD)	81.7 (20.6)	83.2 (20.0)	102.4 (33.2)	78.1 (7.1)	72.7 (10.5)	78.8 (25.1)	82.1 (16.2)	86.4 (20.1)	83.2 (20.3)
Median	84.6	82.6	89	78.4	70.8	71.8	80.1	84.5	80.1
Range	45–102	66–102	72–147	67–88	63–87	56–126	62–99	67–123	45–147
Baseline KPS									
70	1	0	1	0	1	2	3	1	9
80	4	1	1	1	1	3	0	2	13
90	2	3	3	5	2	2	4	3	24
100	0	0	0	0	0	0	1	0	1

MRI and PET acquisition

All study patients received baseline MRI and PET scans on approved 1.5T and 3T MRI scanners 14 days prior to initiation of study drug while either not receiving glucocorticoids or on a stable dose (i.e., same daily dose) of glucocorticoids during the 5 consecutive days prior to the baseline scan. MRI and PET scanners were approved by an independent radiological facility (MedQIA) based on (i) adherence to the targeted acquisition parameters including image resolution ($\pm 10\%$); (ii) qualitative assessments of image quality to look for motion artifacts, geometric distortions, etc.; and (iii) adequate range of quantitative measures in normal-appearing tissue (e.g., T1 and ADC measurements, etc.) both submitted MRI and PET phantoms (for conditional approval) as well as patient examinations (for full approval). The first follow-up time point was within 2 weeks after the first dose of GDC-0084 in 7 of the 47 patients, spread across various dose levels, and 1–2 months after the first dose in 38 of the patients, with 2 patients not having any follow-up evaluations. Follow-up images were acquired on the same accredited MRI and PET scanners used at baseline. The MRI protocol (Supplementary Table S1) consisted of axial T2-weighted images, axial T2-weighted FLAIR images, axial 30 direction diffusion tensor images (DTI), 2-point Dixon VIBE sequence for attenuation correction on MR-PET scanners (24), axial precontrast T1-weighted turbo spin echo (TSE) images, axial variable flip angle 3D gradient echo (GRE) images for precontrast T1 mapping, axial dynamic contrast enhanced (DCE) perfusion MRI images obtained with a single dose of contrast, axial dynamic susceptibility contrast (DSC) perfusion MRI obtained after a second dose of contrast (using the DCE dose as a preload of contrast), parameter-matched postcontrast axial T1-weighted TSE images, and a 1–1.5 mm isotropic resolution postcontrast 3D T1-weighted inversion recovery prepared gradient echo (IR-GRE) sequence. Supplementary Table S1 outlines the general MRI protocol sequence parameters for 3T.

^{18}F -FDG was synthesized using standard methods (25, 26) to an average specific radioactivity of 200 GBq/mmol. PET scans were acquired 60 minutes after injection of 2.0 MBq/kg body weight of ^{18}F -FDG, administered as an isotonic neutral solution. A total of 30 minutes of PET data acquisition was acquired with the PET scanner in 3D mode (average of 6 frames \times 5 minutes). At the end of PET image acquisition, a transmission scan was acquired to correct for photon attenuation (for CT/PET scans). PET emission data was corrected for photon attenuation, photon scatter, and random coincidences, and then reconstructed using a standard filtered backprojection technique and a Hanning filter with cut-off frequency of 0.5 cycles per bin, yielding a full-width half-maximum of 5 mm.

Figure 1 illustrates the available data used for this study. A total of 27 of the 47 patients enrolled received ^{18}F -FDG PET and multi-parametric MRI prior to and following cycle 2 of GDC-0084, while 34 of the 47 patients received DCE and DSC perfusion MRI. The remaining 10 patients received anatomic MRI, DSC perfusion MRI, and diffusion tensor imaging (DTI) or diffusion-weighted imaging (DWI) prior to and after administration of GDC-0084, along with every 2 cycles until tumor recurrence or death. Of these patients with available data (outlined in **Fig. 1**), a subset of high-quality posttreatment imaging data and another subset of high-quality matched pretreatment and posttreatment imaging data were used for subsequent analysis. Data were excluded if there was no measurable enhancing disease, artifacts relating to excessive patient motion, artifacts due to geometric distortions, signal dropout, incomplete enhancing tumor coverage, corrupt raw data files, incorrect acquisition parameters (outside a range of $\sim 10\%$ variation), patient intolerability

or claustrophobia, unavailability of tracers, or technical issues during image acquisition.

MRI and PET postprocessing

Definition of enhancing tumor

Contrast-enhanced T1-weighted subtraction maps (**Fig. 2**) were created using parameter matched pre- and postcontrast axial 2D T1-weighted images and techniques described previously (27–29). These images were then registered to 3D 1–1.5 mm isotropic postcontrast T1-weighted images for a common patient reference. Tumor volumes of interest (VOI) were created and included areas of contrast enhancement on T1 subtraction maps and excluded central necrosis as defined hypointensity on T1 postcontrast and subtraction maps, surrounded by contiguous enhancing disease.

^{18}F -FDG

Standardized uptake value (SUV) maps were calculated (30) and registered to 3D postcontrast T1-weighted images. ^{18}F -FDG SUV within enhancing tumor (defined above) and within a 10 mm spherical volume placed in the contralateral hemisphere within normal-appearing white matter (NAWM) were measured. The median ratio of ^{18}F -FDG uptake in enhancing tumor to NAWM within the enhancing tumor was calculated and used in subsequent analyses.

Diffusion imaging

Apparent diffusion coefficient (ADC) was estimated as the mean diffusivity on DTI or DWI images and fractional anisotropy (FA) measurements were created (31, 32). Median ADC and FA within enhancing tumor (defined above) were then calculated for each patient after registration to patient-specific 3D postcontrast T1-weighted images.

Perfusion MRI

Precontrast T1 maps were calculated using variable flip angle data and nonlinear regression in MATLAB (Version 2018a, The MathWorks, Inc.). Estimates of K^{trans} , the flux rate of contrast from the intravascular to extravascular space often as a surrogate for vascular permeability (33, 34), and the plasma volume fraction, v_p , were estimated using the Extended Tofts model (35) applied to DCE-MRI data. Estimates of relative cerebral blood volume (rCBV) were obtained using a bidirectional leakage correction algorithm (36, 37) applied to DSC-MRI data. The median ratio of rCBV within the enhancing tumor to NAWM (defined as 10 mm diameter sphere in the contralateral hemisphere) along with median K^{trans} and v_p within enhancing tumor were estimated and used in subsequent analyses.

Pharmacokinetic analysis

To determine the single-dose pharmacokinetic (PK) properties of GDC-0084, frequent blood sampling through 24 hours was obtained following a single dose of GDC-0084 administered orally on Day 1 of Cycle 1. A validated LC/MS-MS assay with a lower level of quantification (LLOQ) of 0.00052 $\mu\text{mol/L}$ was used to quantify the concentration of GDC-0084 in plasma samples. Nominal time data were used in the analysis, and the linear up/log down trapezoidal method was used for calculating the area under the concentration–time curve (AUC). All plasma concentration–time data collected in Cycle 1 were analyzed using WinNonlin (Version 6.4, Pharsight Corp) to estimate PK parameters, which included but were not limited to AUC and C_{max} .

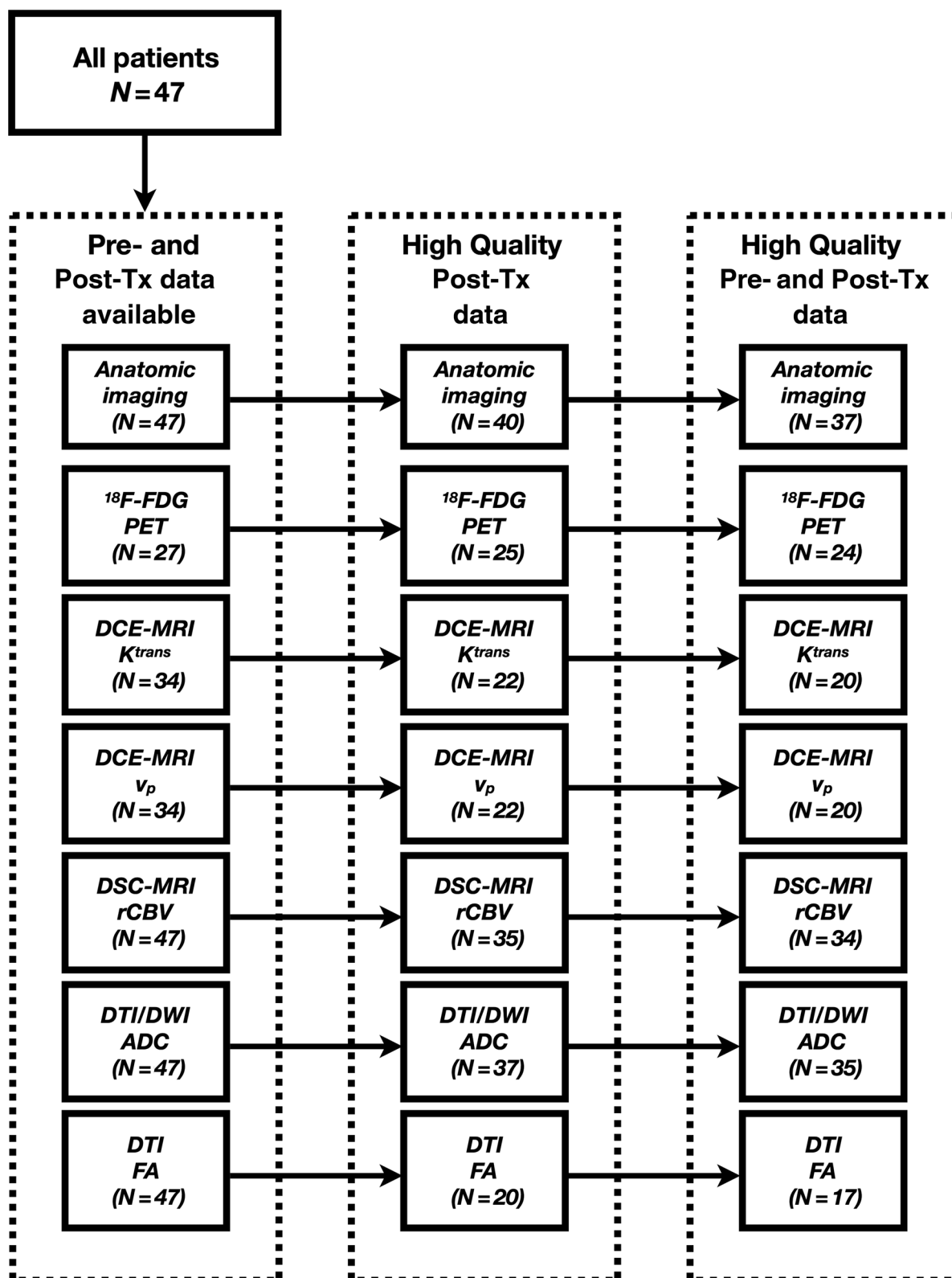


Figure 1.

Data flow diagram describing available imaging data for each parameter. A total of 47 patients were enrolled in this trial. Of which, all patients had anatomic imaging, but only a subset of patients had MRI and PET imaging data available and of sufficient quality for this study.

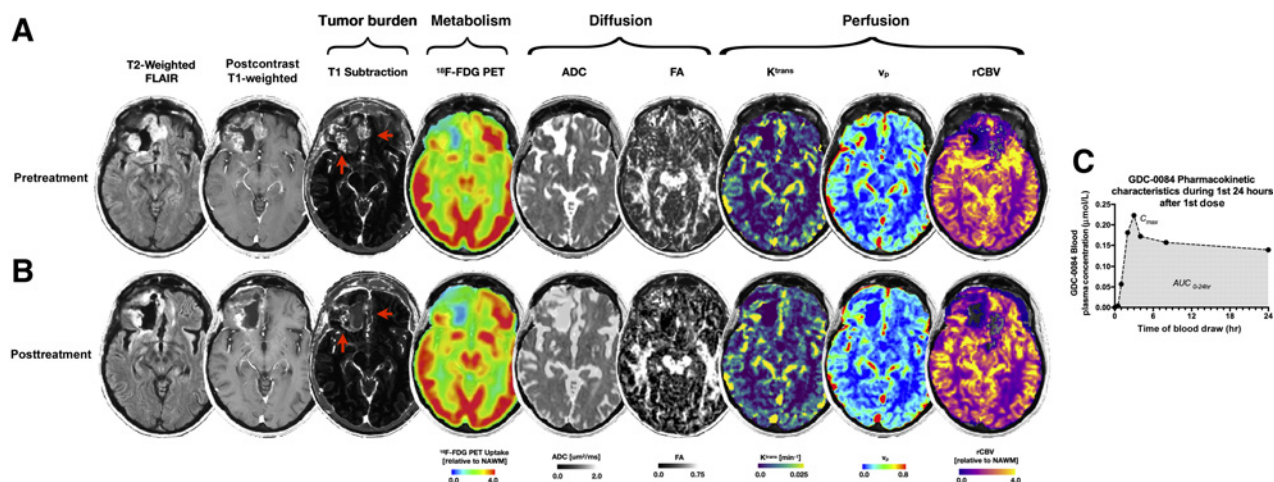


Figure 2.

Example MR-PET imaging response in a 47-year-old female patient with recurrent glioblastoma treated with 45 mg of GDC-0084. Baseline, pretreatment (**A**) and 2-month posttreatment (**B**) multiparametric MR-PET images are shown, including T2-weighted fluid attenuated inversion recovery (FLAIR), postcontrast T1-weighted images, T1 digital subtraction maps, normalized ^{18}F -FDG PET SUV maps fused to anatomic MR images, ADC maps, FA maps, as well as maps of K^{trans} , plasma volume fraction (v_p), and rCBV. **C**, Pharmacokinetic characteristics during the first 24 hours after the 1st dose of GDC-0084 in this patient. Red arrows show reduction in contrast-enhancing tumor burden after treatment.

Data and statistical analysis

The percentage change in median values of multiparametric MR-PET imaging parameters within contrast-enhancing tumor were evaluated per oral dose (2 mg–65 mg). A correlation matrix was calculated for the percentage change in imaging measurements to understand the interrelationship between the different MR-PET imaging parameters. All MR-PET imaging parameters were then independently correlated with C_{max} and AUC from PK evaluation to explore any associations using a level of significance, $\alpha = 0.05$, not correcting for any multiple comparisons. Because not all patients had a full set of multiparametric MR-PET imaging measurements, piecewise cubic spline interpolation was used to impute missing data via MATLAB (Version 2018a, The MathWorks, Inc.). A set of multivariable linear regression models based on imputed multiparametric MR-PET imaging measurements were then trained to predict PK parameters C_{max} and AUC. Model predictions of C_{max} and AUC were then subsequently used to predict radiographic PFS in patients who progressed on study (41 of 47 patients) using univariate log-rank analyses applied to Kaplan–Meier data.

Results

At study enrollment, 33 patients (70.2%) were classified as having glioblastoma (WHO IV) while 14 patients (29.8%) had WHO grade III malignant gliomas. The median time from primary diagnosis was 40.5 months, and the median number of prior surgeries was 2.0 (range 1–6) and median number of prior systemic therapies was 3.0 (range 1–5). Investigator-assessed RANO (38) evaluations in this phase I dose-escalation study suggested the best overall response was 40.4% of patients with stable disease (19 of 47), while 55.3% of patients (26 of 47) experienced rapid disease progression and the remaining patients were not evaluable. A linear trend was observed between the proportion of patients with stable disease at each dose level and the oral dose ($R^2 = 0.6362$; $P = 0.0177$), as 28.6% of patients treated with 2 mg had stable disease, 25% at 4 mg, 40% at 8 mg, 33.3% at 15 mg, 25% at 20 mg, 42.9% at 30 mg, 37.5%

at 45 mg, and 83.8% of patients (5 of 6) had stable disease at the highest dose level of 65 mg. **Figure 2** illustrates an example of a 47-year-old female patient with complete multiparametric MR-PET imaging treated with an oral dose of 45 mg of GDC-0084, demonstrating reduction in contrast-enhancing tumor burden along with changes in multiparametric MR-PET images. Seven of the 27 patients had visible, measurable metabolic response on ^{18}F -FDG PET SUV images according to independent radiological facility determination (see Supplementary Fig. S1 for examples). Thirty-seven patients (78.7%) were on-study for less than 3 months, 7 patients (14.9%) were on-study for 3–6 months, and 3 patients (6.4%) were on-study for 6–12 months.

Correlation between MR-PET imaging measurements

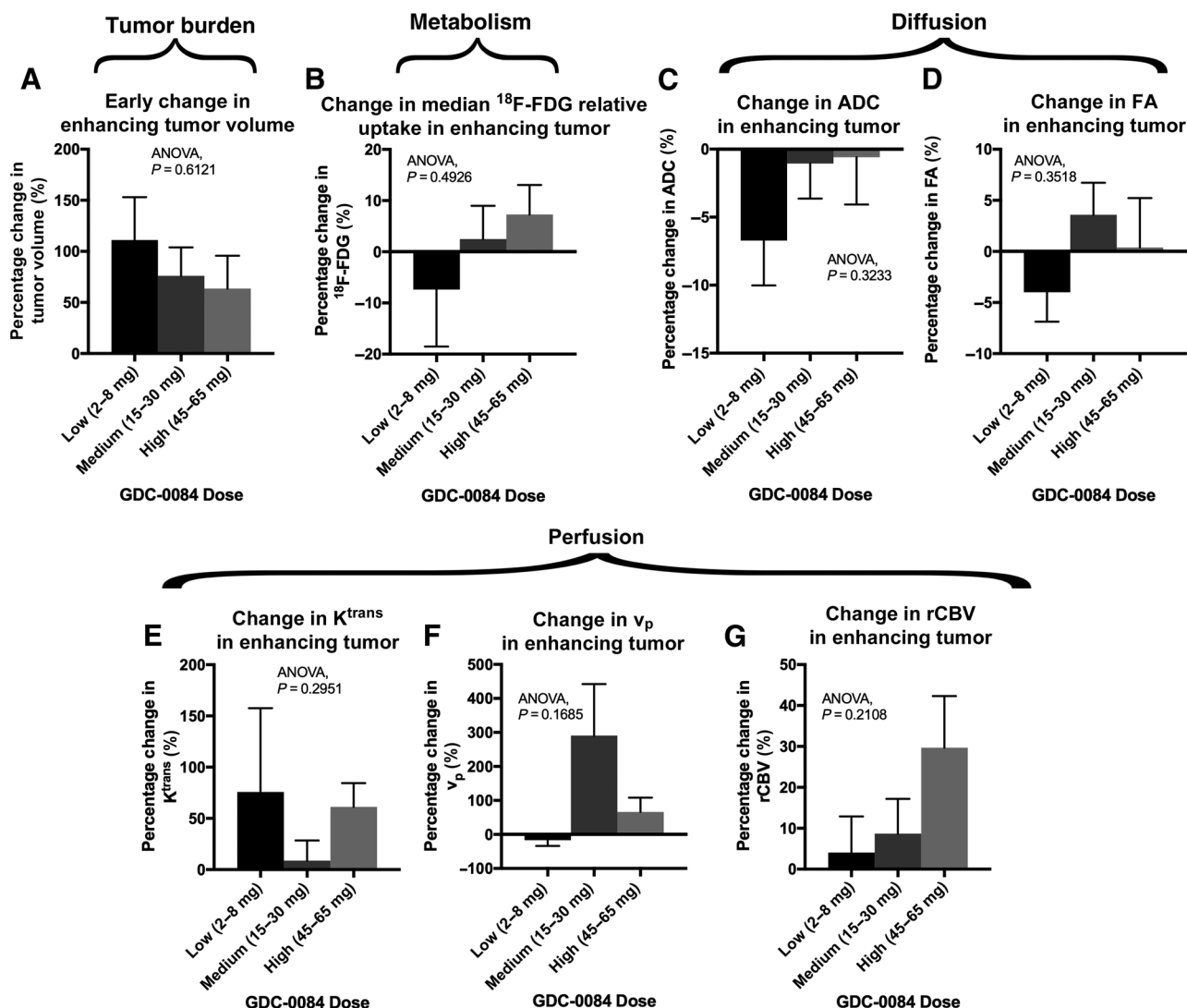
No significant correlations were observed between measurements of change in multiparametric MR-PET imaging measurements before and after treatment (Supplementary Fig. S2; $P > 0.05$), suggesting these measurements reflect independent characteristics of physiologic behavior.

Dose-dependent posttreatment changes MR-PET imaging

No statistically significant dose-dependent differences were observed when comparing change in enhancing tumor volume (**Fig. 3A**; $P = 0.6121$), ^{18}F -FDG uptake (**Fig. 3B**; $P = 0.4926$), ADC (**Fig. 3C**; $P = 0.3233$), FA (**Fig. 3D**; $P = 0.3518$), K^{trans} (**Fig. 3E**; $P = 0.2951$), v_p (**Fig. 3F**; $P = 0.1685$), or rCBV (**Fig. 3G**; $P = 0.2108$) across low, medium, and high doses (see Supplementary Fig. S3 for data on individual dose levels and patient cohorts).

Multiparametric MR-PET imaging prediction of C_{max}

A significant negative correlation was observed between change in enhancing tumor volume and C_{max} (**Fig. 4A**; $R^2 = 0.1295$; $P = 0.0287$), while a significant positive association was observed between C_{max} and both change in FA (**Fig. 4D**; $R^2 = 0.2482$; $P = 0.0418$) and v_p (**Fig. 4F**; $R^2 = 0.3919$; $P = 0.0032$). No significant linear associations were observed between C_{max} and percentage change in ^{18}F -FDG uptake,

**Figure 3.**

Multiparametric MR-PET imaging responses for various oral dose levels of GDC-0084. Change in contrast-enhancing tumor volume (A), median ^{18}F -FDG uptake relative to white matter (B), median ADC (C), median FA (D), median K^{trans} (E), median v_p (F), and median rCBV for low (2-8 mg), medium (15-30 mg), and high (45-65 mg) oral dose levels of GDC-0084 (G).

ADC, K^{trans} , or rCBV. A multivariable linear regression model could estimate, but tended to slightly underestimate, measured C_{max} (Fig. 4H; $R^2 = 0.4113$; $P < 0.0001$). Supplementary Table S2 outlines the specific model parameters.

Multiparametric MR-PET imaging prediction of AUC

Next, the relationship between MR-PET imaging measurements and AUC during the first 24 hours were explored. A strong association was observed between C_{max} and AUC (Supplementary Fig. S4; $R^2 = 0.8794$; $P < 0.0001$). No significant correlations were observed between the percentage change in MR-PET measurements after GDC-0084 and measured AUC (Fig. 5); however, a decrease in contrast-enhancing tumor volume (Fig. 5A; $R^2 = 0.1035$; $P = 0.0522$), increase in FA (Fig. 5D; $R^2 = 0.2003$; $P = 0.0716$), and increase in v_p (Fig. 5F; $R^2 = 0.1917$; $P = 0.0535$) trended toward a higher AUC. A multivariate linear regression model created from

MR-PET imaging measurements within contrast-enhancing tumor before and after the first dose of GDC-0084 was able to predict AUC within the first 24 hours (Fig. 5H; $R^2 = 0.3421$; $P < 0.0001$). Supplementary Table S3 outlines the specific model parameters.

Association between multiparametric MR-PET imaging and PFS

The linear regression models created from MR-PET imaging measurements were used to determine whether estimates of C_{max} or AUC could be used to predict PFS in patients who continued to receive drug until radiographic progression (41 of 47). Using an empirical threshold of $C_{\text{max}} = 0.1 \mu\text{mol/L}$, which was approximately the cohort median measured C_{max} , a linear combination of multiparametric MR-PET imaging measurements before and after GDC-0084 could be used to stratify long and short PFS (Fig. 6A; log-rank $P = 0.0039$; HR = 0.4176). Similarly, model estimate of $\text{AUC} = 1.25 \mu\text{mol/L} \times \text{hour}$ estimated from a linear combination of

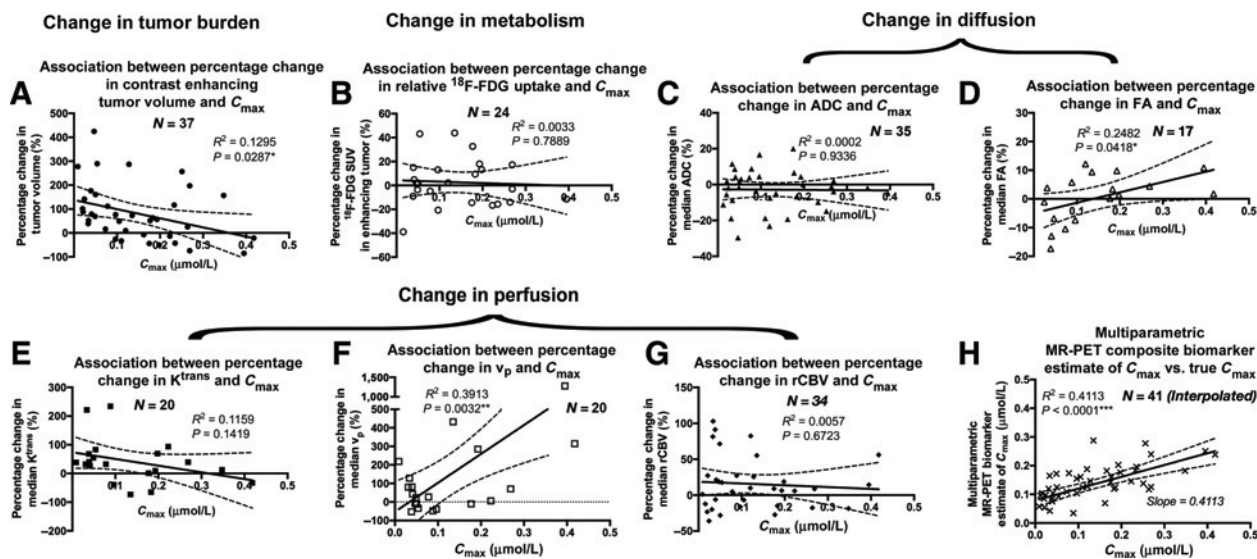


Figure 4.

Correlation between multiparametric MR-PET imaging responses and C_{max} . Correlation between measured C_{max} and change in contrast-enhancing tumor volume (A), median ^{18}F -FDG uptake relative to white matter (B), median ADC (C), median FA (D), median K^{trans} (E), median v_p (F), and median rCBV (G). H, Model predictions of C_{max} using a linear combination of multiparametric MR-PET imaging measurements compared with measured values of C_{max} .

MR-PET measurement responses could predict PFS (Fig. 6B; log-rank $P = 0.0296$; HR = 0.4679). Interestingly, measured C_{max} from blood was not proportional to PFS (Cox Univariate $P = 0.6162$) and a similar threshold of $C_{max} = 0.1 \mu\text{mol/L}$ did not result in a difference in PFS (Fig. 6C; log-rank $P = 0.8111$). Similarly, measured AUC was not proportional to PFS (Cox Univariate $P = 0.6168$) and grouping patients based on a measured AUC = $1.25 \mu\text{mol/L} \times \text{hour}$ did not show a significant difference in PFS (Fig. 6D; log-rank $P = 0.5977$).

Additional observations

In addition to changes in multiparametric MR-PET, we observed a statistically significant association between C_{max} and posttreatment measurements of contrast-enhancing tumor burden (Supplementary Fig. S5A; $R^2 = 0.1304$; $P = 0.0221$), ^{18}F -FDG uptake (Supplementary Fig. S5B; $R^2 = 0.1902$; $P = 0.0293$), K^{trans} (Supplementary Fig. S5C; $R^2 = 0.3046$; $P = 0.0078$), and rCBV (Supplementary Fig. S5D; $R^2 = 0.1649$; $P = 0.0155$).

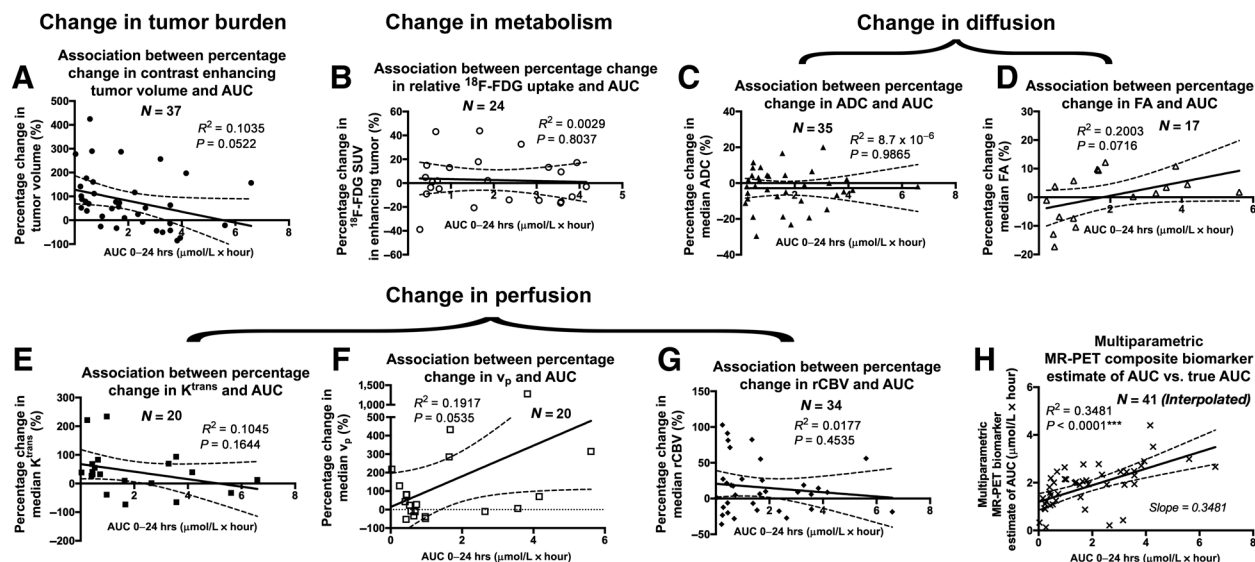
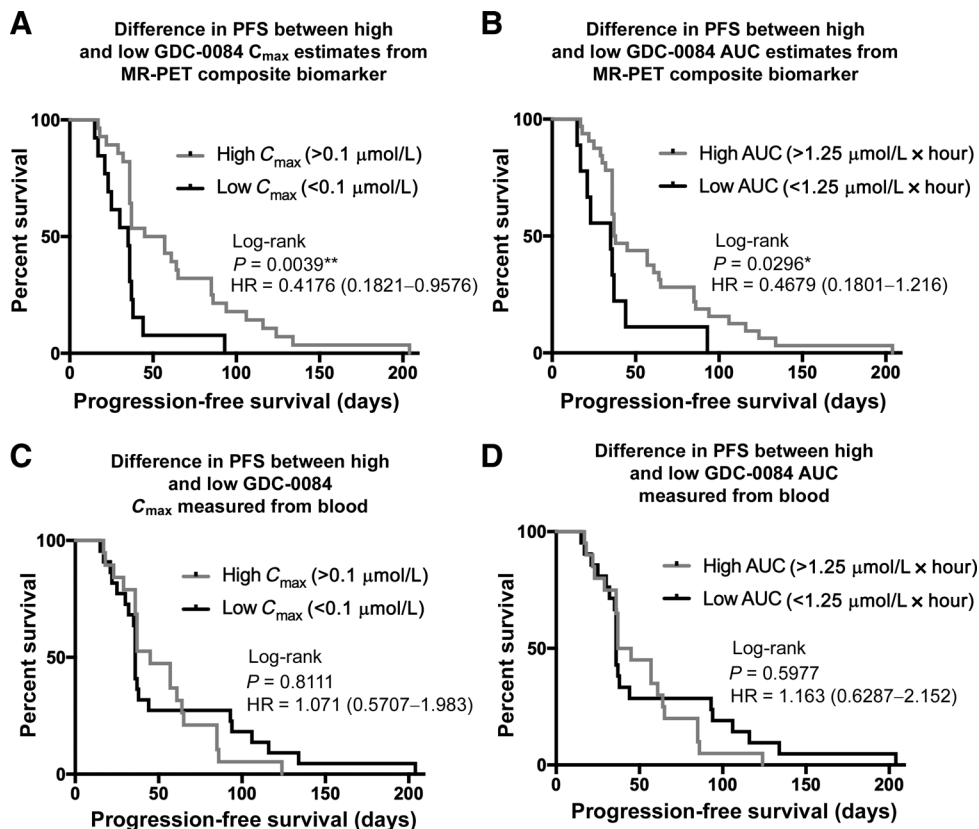


Figure 5.

Correlation between multiparametric MR-PET imaging responses and AUC. Correlation between measured AUC and change in contrast-enhancing tumor volume (A), median ^{18}F -FDG uptake relative to white matter (B), median ADC (C), median FA (D), median K^{trans} (E), median v_p (F), and median rCBV (G). H, Model predictions of AUC using a linear combination of multiparametric MR-PET imaging measurements compared with measured values of C_{max} .

**Figure 6.**

Difference in PFS between multiparametric MR-PET imaging estimates of high and low concentration and exposure to GDC-0084. **A**, Difference in PFS between imaging estimates of high C_{max} ($>0.1 \mu\text{mol/L}$) and low C_{max} ($<0.1 \mu\text{mol/L}$; log-rank $P = 0.0039$). **B**, Difference in PFS between imaging estimates of high AUC ($>1.25 \mu\text{mol/L} \cdot \text{hour}$) and low AUC ($<1.25 \mu\text{mol/L} \cdot \text{hour}$; log-rank $P = 0.0296$). **C**, Difference in PFS between blood estimates of high C_{max} ($>0.1 \mu\text{mol/L}$) and low C_{max} ($<0.1 \mu\text{mol/L}$; log-rank, $P = 0.8111$). **D**, Difference in PFS between blood estimates of high AUC ($>1.25 \mu\text{mol/L} \cdot \text{hour}$) and low AUC ($<1.25 \mu\text{mol/L} \cdot \text{hour}$; log-rank, $P = 0.5977$).

Discussion

Although the PI3K pathway is altered in more than 80% of glioblastoma, many have questioned the ability to target this pathway based on the large number of failed clinical trials (39). GDC-0084 was specifically optimized to cross the blood–brain barrier while maintaining adequate potency and selectivity (14). *In vitro* and preclinical studies have demonstrated efficacy and brain penetration of GDC-0084 (40), suggesting this agent may demonstrate activity in human glioblastoma. Because successful mTOR (17–19) and PI3K inhibition (20–22) are thought to reduce glucose utilization and reduce tumor vascularity, respectively, we hypothesized multiparametric MR-PET imaging using a combination of ^{18}F -FDG PET, along with diffusion and perfusion MRI, may be useful for noninvasively characterizing the multifaceted response to GDC-0084 in patients with malignant gliomas and potentially useful for predicting drug concentration and exposure.

Results from this study appear to at least partially support this hypothesis, although individual imaging measurements showed mostly trends and the individual comparisons were not corrected for multiple testing. There appeared to be trends toward dose-dependent effects of GDC-0084 on the volume of contrast enhancement, indicating that change in enhancing tumor burden remains an important measurement of drug efficacy (41). Similar to reductions in contrast-enhancing tumor burden, estimates of K^{trans} , often used as a surrogate for vascular permeability, also trended toward a reduction in proportion to C_{max} , supporting the notion that PI3K inhibition using GDC-0084 would result in reduction in abnormal vascularity or vascular characteristics. Results also suggested an increase in FA may be associated with higher drug concentrations and exposure. This may

suggest reduction in edema and reemergence of white matter fibers within edematous tissue after treatment with GDC-0084. Surprisingly, no strong association was observed between change in ^{18}F -FDG uptake and PK parameters. This may be due, in part, to the fact that ^{18}F -FDG SUV measurement during static PET scanning reflects accumulation of ^{18}F -FDG, the mechanisms of which are complex (42–44) and include both tumor-related (e.g., glucose metabolism, vascular fraction, tumor size, hypoxia, etc.) and nontumor-related mechanisms (e.g., high-serum glucose, inflammation, etc.). It is important to note that we did observe global decreases in ^{18}F -FDG uptake in many patients as illustrated in Supplementary Fig. S1C and S1E, which may suggest brain penetration and mTOR inhibition throughout the brain. In addition, a correlation between C_{max} and posttreatment estimates of ^{18}F -FDG, tumor volume, K^{trans} , and rCBV (Supplementary Fig. S5) were detected, which appears consistent with our original hypotheses.

Because repeated brain surgeries are not realistic to quantify drug penetration in most patients with malignant glioma and traditional PK studies and “phase 0” or “window of opportunity” studies can be both time-consuming and expensive, there remains an unmet need in neuro-oncology for noninvasive biomarkers that can be used to estimate drug PK characteristics.

In this study we created a simple model for predicting both C_{max} and AUC using a linear combination of all available multiparametric MR-PET imaging parameters. Then, using the noninvasive imaging estimates of drug concentration and exposure, we were able to predict patients with more favorable PFS. While preliminary results from this study suggest composite biomarkers created from multiparametric MR-PET imaging targeting metabolic and/or physiologic processes specific to the drug mechanism of action may be useful for subsequent

evaluation of treatment efficacy in larger phase II–III studies. And while machine learning and artificial intelligence techniques hold the promise of similarly predicting features like drug penetration and outcome using noninvasive imaging information, these approaches require large amounts of data to generalize these characteristics, which will not be available when testing novel drugs. Thus, this study suggests a simple linear combination of multiparametric MRI and PET imaging measurements can effectively predict PK parameters and PFS. Interestingly, actual measures of drug concentration and exposure from blood did not appear to predict PFS, suggesting that estimations of exposure using a combination of imaging features may provide added value over direct blood PK measurements. It is conceivable this may be due, in part, to changes in imaging measurements reflecting drug penetration and target engagement in individual patients as opposed systemic drug exposure, although this is only speculative.

There are a number of important limitations to this study that should be addressed. First, no multiple comparisons corrections were performed when evaluating the correlation between PK parameters and multiple imaging measurements. Because we did not observe a strong correlation between the various imaging measurements and because this was a small pilot study, we felt as though a conservative approach to correcting for multiple comparisons (e.g., Bonferroni correction) would inhibit our ability to identify potentially meaningful associations between individual imaging measurements and PK parameters. Future studies with more patients and a targeted small number of specific imaging measurements may be useful for refining these associations. Second, despite great efforts to standardize image acquisition, there were a large variety in ^{18}F -FDG PET SUV measurements in both phantom calibration (results not shown) as well as in tumor and normal brain tissue. To overcome these challenges, we chose to normalize ^{18}F -FDG uptake in the enhancing tumor to that of normal white matter. However, as illustrated in Supplementary Fig. S1C and S1E, global changes in ^{18}F -FDG uptake may occur and may actually reflect brain penetration of GDC-0084 and meaningful inhibition of mTOR. Thus, more sophisticated techniques for isolating the changes in ^{18}F -FDG metabolism within the tumor from that of background tissue, or even considering global changes in glucose utilization as a potentially meaningful indicator of mTOR inhibition, may be important. Similarly, despite great efforts to standardize acquisition of DTI and perfusion MRI, some studies were not in compliance and were not usable in subsequent analyses. Consequently, not all patients had all imaging measurements available, therefore results should be interpreted with caution and findings should be replicated in an independent cohort. Also, greater efforts to balance the needed complexity of multiparametric MR-PET imaging studies with what is practical at various sites is critical to ensure similarly designed trials can quantify needed parameters while maximizing the amount of available data. Finally, the patients in this trial were heavily pretreated and therefore the single-agent antitumor activity may have been significantly limited. It is conceivable that GDC-0084 may have more clinical activity in patients who are less heavily treated or in the first-line setting where tumors are less heterogeneous and aggressive.

Another vital set of limitations that should be addressed is the assumption that a favorable blood PK is closely linked with tissue PK/PD and that favorable tissue PK/PD is necessary to cause a tumor response. While we rationalized that a favorable blood PK is a necessary, but not sufficient, condition for a physiologic drug effect, tissue drug concentrations and biological effects depend on a number of complex characteristics including properties of the particular drug, regional perfusion, blood clearance, drug metabolism, and genetic or epigenetic differences within the tumor. It is conceivable that these

complex interactions were responsible for some of the variability we observed when relating imaging parameters with PK measurements as well as our observations that blood PK was not directly predictive of PFS, whereas imaging response which presumably reflected biological changes imposed by direct target engagement by the drug, was predictive of PFS. Thus, results from this study should be interpreted with some caution until more comprehensive studies have been conducted to isolate these specific effects.

Conclusions

A combination of multiparametric MR-PET imaging parameters aimed to targeting metabolic and physiologic changes resulting from mTOR and PI3K inhibition can be used to estimate GDC-0084 pharmacokinetics and predict PFS in patients with recurrent high-grade gliomas.

Disclosure of Potential Conflicts of Interest

B.M. Ellingson is an employee/paid consultant for MedQia, Genentech/Roche, Agios Pharmaceuticals, Siemens, Janssen, Medicenna, Imaging Endpoints, Kazia Therapeutics, Northwest Biopharmaceuticals, Oncocetics, Beigene, and VBL Therapeutics, and reports receiving commercial research grants from Janssen, Siemens and VBL Therapeutics. J. Simpson is an employee/paid consultant for Kazia Therapeutics and holds ownership interest (including patents) in Bionomics Ltd. J.S. Garner is an employee/paid consultant for and holds ownership interest (including patents) in Kazia Therapeutics Limited. A.G. Olivero is an employee/paid consultant for Genentech/Roche, Kazia, Aduro, ORIC, and Imugene, and holds ownership interest (including patents) in Roche. L.U. Mueller is an employee/paid consultant for Genentech. E. Gerstner is an employee/paid consultant for Blue Earth Diagnostics. T.F. Cloughesy is an employee/paid consultant for Roche, Trizel, Medscape, Bayer, Amgen, Del Mar Pharmaceuticals, Tocagen, Karyopharm, GW Pharma, Odonate Therapeutics, Pascal Biosciences, Kiyatec, AbbVie, Boehringer Ingelheim, VBI, Deciphera, VBL, Agios, Merck, Genocera, Celgene, Puma, Lilly, BMS, Cortice, Wellcome Trust, Novocure, Novogen, Boston Biomedical, Sunovion, Human Longevity, Insys, ProNai, Pfizer, Notable Labs, MedQia, reports receiving speakers bureau honoraria from Roche, holds ownership interest (including patents) in Katmai Pharmaceuticals, is an advisory board member/unpaid consultant for Global Coalition for Adaptive Research, and has a patent on brain penetrant targeted therapy owned by UCLA and licensed by Katmai Pharmaceuticals. P.Y. Wen is an employee/paid consultant for Bayer, Blue Earth Diagnostics, Deciphera, Elevate Bio, Imvax, Integral Health, Karyopharm, Kiyatec, VBI Vaccines, reports receiving commercial research grants from Genentech/Roche, MediciNova, Sanofi-Aventis, VBI Vaccines, and reports receiving speakers bureau honoraria from Prime Oncology. No potential conflicts of interest were disclosed by the other authors.

Authors' Contributions

Conception and design: B.M. Ellingson, J. Simpson, J.S. Garner, A.G. Olivero, L.U. Mueller, J. Rodon, T.F. Cloughesy, P.Y. Wen

Development of methodology: B.M. Ellingson, T.F. Cloughesy, P.Y. Wen

Acquisition of data (provided animals, acquired and managed patients, provided facilities, etc.): B.M. Ellingson, J. Simpson, J. Rodon, E. Gerstner, T.F. Cloughesy, P.Y. Wen

Analysis and interpretation of data (e.g., statistical analysis, biostatistics, computational analysis): B.M. Ellingson, J. Yao, D.A. Nathanson, A. Chakhoyan, J. Simpson, L.U. Mueller, E. Gerstner, P.Y. Wen

Writing, review, and/or revision of the manuscript: B.M. Ellingson, J. Yao, J. Simpson, J.S. Garner, A.G. Olivero, J. Rodon, E. Gerstner, T.F. Cloughesy, P.Y. Wen

Administrative, technical, or material support (i.e., reporting or organizing data, constructing databases): B.M. Ellingson, C. Raymond, J. Simpson, J.S. Garner

Study supervision: L.U. Mueller, E. Gerstner

The costs of publication of this article were defrayed in part by the payment of page charges. This article must therefore be hereby marked advertisement in accordance with 18 U.S.C. Section 1734 solely to indicate this fact.

Received November 23, 2019; revised February 14, 2020; accepted April 3, 2020; published first April 8, 2020.

References

- Stupp R, Taillibert S, Kanner A, Read W, Steinberg D, Lhermitte B, et al. Effect of tumor-treating fields plus maintenance temozolomide vs. maintenance temozolomide alone on survival in patients with glioblastoma: a randomized clinical trial. *JAMA* 2017;318:2306–16.
- Stupp R, Mason WP, van den Bent MJ, Weller M, Fisher B, Taphoorn MJ, et al. Radiotherapy plus concomitant and adjuvant temozolomide for glioblastoma. *N Engl J Med* 2005;352:987–96.
- Chinot OL, Wick W, Mason W, Henriksson R, Saran F, Nishikawa R, et al. Bevacizumab plus radiotherapy-temozolomide for newly diagnosed glioblastoma. *N Engl J Med* 2014;370:709–22.
- Brennan CW, Verhaak RG, McKenna A, Campos B, Noushmehr H, Salama SR, et al. The somatic genomic landscape of glioblastoma. *Cell* 2013;155:462–77.
- Raizer JJ, Abrey LE, Lassman AB, Chang SM, Lamborn KR, Kuhn JG, et al. A phase II trial of erlotinib in patients with recurrent malignant gliomas and nonprogressive glioblastoma multiforme postradiation therapy. *Neuro Oncol* 2010;12:95–103.
- Thiessen B, Stewart C, Tsao M, Kamel-Reid S, Schaiquevich P, Mason W, et al. A phase I/II trial of GW572016 (lapatinib) in recurrent glioblastoma multiforme: clinical outcomes, pharmacokinetics and molecular correlation. *Cancer Chemother Pharmacol* 2010;65:353–61.
- Chinnaiyan P, Won M, Wen PY, Rojiani AM, Wendland M, Dipetrillo TA, et al. RTOG 0913: a phase I study of daily everolimus (RAD001) in combination with radiation therapy and temozolomide in patients with newly diagnosed glioblastoma. *Int J Radiat Oncol Biol Phys* 2013;86:880–4.
- Uhm JH, Ballman KV, Wu W, Giannini C, Krauss JC, Buckner JC, et al. Phase II evaluation of gefitinib in patients with newly diagnosed Grade 4 astrocytoma: Mayo/North central cancer treatment group study N0074. *Int J Radiat Oncol Biol Phys* 2011;80:347–53.
- Franceschi E, Cavallo G, Lonardi S, Magrini E, Tosoni A, Grosso D, et al. Gefitinib in patients with progressive high-grade gliomas: a multicentre phase II study by gruppo italiano cooperativo di neuro-oncologia (GICNO). *Br J Cancer* 2007;96:1047–51.
- de Vries NA, Buckle T, Zhao J, Beijnen JH, Schellens JH, van Tellingen O. Restricted brain penetration of the tyrosine kinase inhibitor erlotinib due to the drug transporters P-gp and BCRP. *Invest New Drugs* 2012;30:443–9.
- Polli JW, Olson KL, Chism JP, John-Williams LS, Yeager RL, Woodard SM, et al. An unexpected synergist role of P-glycoprotein and breast cancer resistance protein on the central nervous system penetration of the tyrosine kinase inhibitor lapatinib (N-{3-chloro-4-[(3-fluorobenzyl)oxy]phenyl}-6-[5-({[2-(methylsulfonyl)ethyl]amino)methyl}-2-furyl]-4-quinazolinamine; GW572016). *Drug Metab Dispos* 2009;37:439–42.
- Chu C, Abbara C, Noel-Hudson MS, Thomas-Bourgneuf L, Gonin P, Farinotti R, et al. Disposition of everolimus in mdr1a-/1b- mice and after a pre-treatment of lapatinib in Swiss mice. *Biochem Pharmacol* 2009;77:1629–34.
- Agarwal S, Sane R, Gallardo JL, Ohlfest JR, Elmquist WF. Distribution of gefitinib to the brain is limited by P-glycoprotein (ABCB1) and breast cancer resistance protein (ABCG2)-mediated active efflux. *J Pharmacol Exp Ther* 2010;334:147–55.
- Heffron TP, Ndubaku CO, Salphati L, Aliche B, Cheong J, Drobnick J, et al. Discovery of clinical development candidate GDC-0084, a brain penetrant inhibitor of PI3K and mTOR. *ACS Med Chem Lett* 2016;7:351–6.
- Salphati L, Heffron TP, Aliche B, Nishimura M, Barck K, Carano RA, et al. Targeting the PI3K pathway in the brain—efficacy of a PI3K inhibitor optimized to cross the blood-brain barrier. *Clin Cancer Res* 2012;18:6239–48.
- Wen PY, Cloughesy T, Olivero AG, Lu X, Mueller L, Coimbra AF, et al. A first-in-human phase I study to evaluate the brain-penetrant PI3K/mTOR inhibitor GDC-0084 in patients with progressive or recurrent high-grade glioma. *J Clin Oncol* 2016;34:2012.
- Kezic A, Popovic L, Lalic K. mTOR inhibitor therapy and metabolic consequences: where do we stand? *Oxid Med Cell Longev* 2018;2018:2640342.
- Mao Z, Zhang W. Role of mTOR in glucose and lipid metabolism. *Int J Mol Sci* 2018;19:2043.
- Festuccia WT, Blanchard PG, Belchior T, Chimin P, Paschoal VA, Magdalon J, et al. PPARgamma activation attenuates glucose intolerance induced by mTOR inhibition with rapamycin in rats. *Am J Physiol Endocrinol Metab* 2014;306:E1046–54.
- Jiang BH, Liu LZ. PI3K/PTEN signaling in angiogenesis and tumorigenesis. *Adv Cancer Res* 2009;102:19–65.
- Soler A, Angulo-Urarte A, Graupera M. PI3K at the crossroads of tumor angiogenesis signaling pathways. *Mol Cell Oncol* 2015;2:e975624.
- Karar J, Maity A. PI3K/AKT/mTOR pathway in angiogenesis. *Front Mol Neurosci* 2011;4:51.
- Wen PY, Cloughesy TF, Olivero AG, Morrissey KM, Wilson TR, Lu X, et al. First-in-human phase I study to evaluate the brain-penetrant PI3K/mTOR inhibitor GDC-0084 in patients with progressive or recurrent high-grade glioma. *Clin Cancer Res* 2020;26:1820–28.
- Eiber M, Martinez-Moller A, Souvatzoglou M, Holzapfel K, Pickhard A, Loffelbein D, et al. Value of a Dixon-based MR/PET attenuation correction sequence for the localization and evaluation of PET-positive lesions. *Eur J Nucl Med Mol Imaging* 2011;38:1691–701.
- Hamacher K, Coenen HH, Stocklin G. Efficient stereospecific synthesis of no-carrier-added 2-[¹⁸F]-fluoro-2-deoxy-D-glucose using aminopolyether supported nucleophilic substitution. *J Nucl Med* 1986;27:235–8.
- Yu S. Review of F-FDG synthesis and quality control. *Biomed Imaging Interv J* 2006;2:e57.
- Ellingson BM, Kim HJ, Woodworth DC, Pope WB, Cloughesy JN, Harris RJ, et al. Recurrent glioblastoma treated with bevacizumab: contrast-enhanced T1-weighted subtraction maps improve tumor delineation and aid prediction of survival in a multicenter clinical trial. *Radiology* 2014;271:200–10.
- Ellingson BM, Abrey LE, Garcia J, Chinot O, Wick W, Saran F, et al. Post-chemoradiation volumetric response predicts survival in newly diagnosed glioblastoma treated with radiation, temozolomide, and bevacizumab or placebo. *Neuro Oncol* 2018;20:1525–35.
- Ellingson BM, Aftab DT, Schwab GM, Hessel C, Harris RJ, Woodworth DC, et al. Volumetric response quantified using T1 subtraction predicts long-term survival benefit from cabozantinib monotherapy in recurrent glioblastoma. *Neuro Oncol* 2018;20:1411–8.
- Thie JA. Understanding the standardized uptake value, its methods, and implications for usage. *J Nucl Med* 2004;45:1431–4.
- Basser PJ, Pierpaoli C. Microstructural and physiological features of tissues elucidated by quantitative-diffusion-tensor MRI. *J Magn Reson B* 1996;111:209–19.
- Basser PJ. Inferring microstructural features and the physiological state of tissues from diffusion-weighted images. *NMR Biomed* 1995;8:333–44.
- Cuenod CA, Balvay D. Perfusion and vascular permeability: basic concepts and measurement in DCE-CT and DCE-MRI. *Diagn Interv Imaging* 2013;94:1187–204.
- Sourbron S, Ingrisch M, Siefert A, Reiser M, Herrmann K. Quantification of cerebral blood flow, cerebral blood volume, and blood-brain-barrier leakage with DCE-MRI. *Magn Reson Med* 2009;62:205–17.
- Tofts PS, Brix G, Buckley DL, Evelhoch JL, Henderson E, Knopp MV, et al. Estimating kinetic parameters from dynamic contrast-enhanced T1-weighted MRI of a diffusible tracer: standardized quantities and symbols. *J Magn Reson Imaging* 1999;10:223–32.
- Leu K, Boxerman JL, Cloughesy TF, Lai A, Nghiemphu PL, Liau LM, et al. Improved leakage correction for single-echo dynamic susceptibility contrast perfusion MRI estimates of relative cerebral blood volume in high-grade gliomas by accounting for bidirectional contrast agent exchange. *AJNR Am J Neuroradiol* 2016;37:1440–6.
- Leu K, Boxerman JL, Lai A, Nghiemphu PL, Pope WB, Cloughesy TF, et al. Bidirectional contrast agent leakage correction of dynamic susceptibility contrast (DSC)-MRI improves cerebral blood volume estimation and survival prediction in recurrent glioblastoma treated with bevacizumab. *J Magn Reson Imaging* 2016;44:1229–37.
- Wen PY, Macdonald DR, Reardon DA, Cloughesy TF, Sorensen AG, Galanis E, et al. Updated response assessment criteria for high-grade gliomas: response assessment in neuro-oncology working group. *J Clin Oncol* 2010;28:1963–72.
- Nichol D, Mellinghoff IK. PI3K pathway inhibition in GBM—is there a signal? *Neuro Oncol* 2015;17:1183–4.
- Salphati L, Aliche B, Heffron TP, Shahidi-Latham S, Nishimura M, Cao T, et al. Brain distribution and efficacy of the brain penetrant PI3K inhibitor GDC-0084 in orthotopic mouse models of human glioblastoma. *Drug Metab Dispos* 2016;44:1881–9.
- Ellingson BM, Wen PY, Cloughesy TF. Evidence and context of use for contrast enhancement as a surrogate of disease burden and treatment response in malignant glioma. *Neuro Oncol* 2018;20:457–71.
- Pauwels EK, Ribeiro MJ, Stoot JH, McCreedy VR, Bourguignon M, Maziere B. FDG accumulation and tumor biology. *Nucl Med Biol* 1998;25:317–22.
- Gillies RJ, Robey I, Gatenby RA. Causes and consequences of increased glucose metabolism of cancers. *J Nucl Med* 2008;49:24S–42S.
- Plathow C, Weber WA. Tumor cell metabolism imaging. *J Nucl Med* 2008;49:43S–63S.

Clinical Cancer Research

Multiparametric MR-PET Imaging Predicts Pharmacokinetics and Clinical Response to GDC-0084 in Patients with Recurrent High-Grade Glioma

Benjamin M. Ellingson, Jingwen Yao, Catalina Raymond, et al.

Clin Cancer Res Published OnlineFirst April 8, 2020.

Updated version	Access the most recent version of this article at: doi: 10.1158/1078-0432.CCR-19-3817
Supplementary Material	Access the most recent supplemental material at: http://clincancerres.aacrjournals.org/content/suppl/2020/04/08/1078-0432.CCR-19-3817.DC1

E-mail alerts [Sign up to receive free email-alerts](#) related to this article or journal.

Reprints and Subscriptions To order reprints of this article or to subscribe to the journal, contact the AACR Publications Department at pubs@aacr.org.

Permissions To request permission to re-use all or part of this article, use this link <http://clincancerres.aacrjournals.org/content/early/2020/05/24/1078-0432.CCR-19-3817>. Click on "Request Permissions" which will take you to the Copyright Clearance Center's (CCC) Rightslink site.